International Journal of Earth Sciences (2018) 107:2337–2355
https://doi.org/10.1007/s00531-018-1601-2

ORIGINAL PAPER

Mineral chemistry and geochemistry of ophiolitic metaultramafics from Um Halham and Fawakhir, Central Eastern Desert, Egypt

Abdel-Aal M. Abdel-Karim[1] · Shehata Ali[2] · Shaimaa A. El-Shafei[1]

Received: 9 December 2017 / Accepted: 28 February 2018 / Published online: 13 March 2018
© Springer-Verlag GmbH Germany, part of Springer Nature 2018

Abstract

This study is focused on ophiolitic metaultramafics from Um Halham and Fawakhir, Central Eastern Desert of Egypt. The rocks include serpentinized peridotites, serpentinites together with talc– and quartz–carbonates. The primary spinel relict is Al–chromite [Cr# > 60], which is replaced by Cr–magnetite during metamorphism. The high Cr# of Al–chromites resembles supra-subduction zone (SSZ) peridotites and suggests derivation from the deeper portion of the mantle section with boninitic affinity. These mantle rocks equilibrated with boninitic melt have been generated by high melting degrees. The estimated melting degrees (~ 19–24%) lie within the range of SSZ peridotites. The high Cr# of spinel and Fo content of olivine together with the narrow compositional range suggest a mantle residual origin. Serpentinized peridotite and serpentinites have low Al_2O_3/SiO_2 ratios (mostly < 0.03) like fore-arc mantle wedge serpentinites and further indicate that their mantle protolith had experienced partial melting before serpentinization process. Moreover, they have very low Nb, Ta, Zr and Hf concentrations along with sub-chondritic Nb/Ta (0.3–16) and Zr/Hf (mostly 1–20) ratios further confirming that their mantle source was depleted by earlier melting extraction event. The high chondrite normalized $(La/Sm)_N$ ratios (average 10) reflect input of subduction-related slab melts/fluids into their mantle source.

Keywords Ophiolite · Fore-arc · Fawakhir · Um Halham · Egypt

Introduction

Peridotites as ultramafic mantle section cropped out at the surface of the Earth can offer important information on the geochemical and geodynamic evolution of the upper mantle (e.g., Sano and Kimura 2007; Dai et al. 2011, 2013; Uysal et al. 2012; Khedr et al. 2014).

The Arabian–Nubian Shield (ANS) marks the northern part of the East African Orogen and was formed close to the end of the Proterozoic due to collision between major fragments of East and West Gondwana and termination of the Mozambique Ocean (Stern 1994; Johnson et al. 2003). Accretion of intra-oceanic island arcs and collision between these arcs and a continental margin produced the ANS and created suture zones outlined by ophiolites (Stern 1994, 1996; Stern et al. 2004). Ophiolite sequences are widely distributed in the central and southern segments of the Eastern Desert (ED) of Egypt (Fig. 1). The complete ophiolite successions (e.g., Wadi Ghadir, Gabal Gerf and Fawakhir) are scarce, whereas the dismembered ophiolitic fragments are several (El-Sharkawy and El-Bayoumi 1979; El-Bayoumi 1980; Shackleton et al. 1980; El-Sayed et al. 1999; Abd El-Rahman et al. 2009a, b; El Bahariya 2008, 2012; Abdel-Karim et al. 2016). Fawakhir ophiolitic complex dates 736.5 ± 1.2 Ma (Andresen et al. 2009).

A SSZ setting of the ED ophiolites is commonly acknowledged (El Bahariya and Arai 2003; Azer and Khalil 2005; Azer and Stern 2007; Ahmed et al. 2012; Abdel-Karim et al. 2016, 2017). However, debate exists on whether they were formed in back-arc or fore-arc settings. A back-arc setting is usually concluded based on the geochemical signatures of the volcanic units of the ophiolite assemblage (El-Sayed et al. 1999; Ahmed et al.

Electronic supplementary material The online version of this article (https://doi.org/10.1007/s00531-018-1601-2) contains supplementary material, which is available to authorized users.

✉ Shehata Ali
shehata.ali@mu.edu.eg

[1] Geology Department, Faculty of Science, Zagazig University, Zagazig 44519, Egypt

[2] Geology Department, Faculty of Science, Minia University, Minia 61519, Egypt

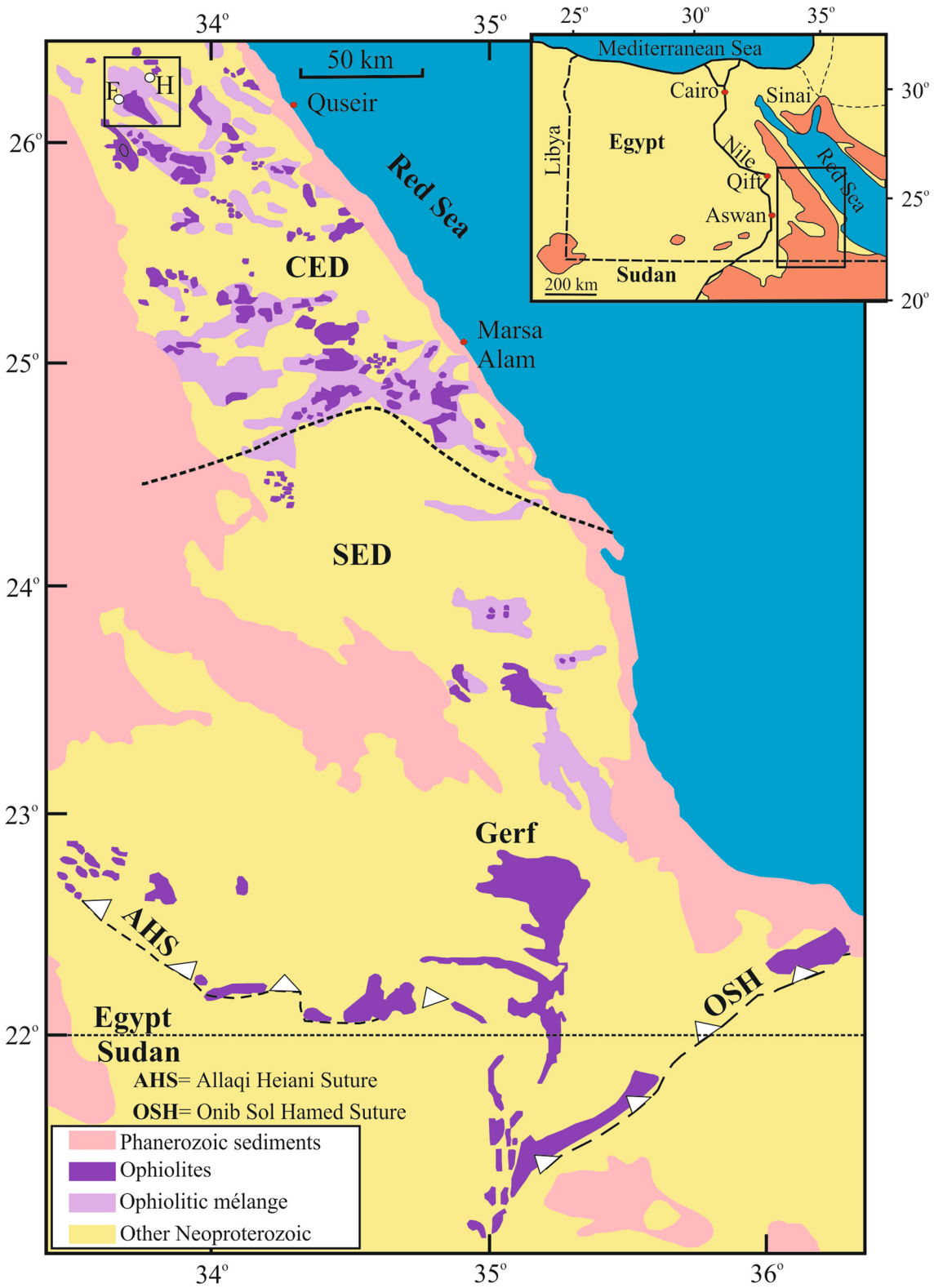

Fig. 1 Ophiolites distribution in the central and southern Eastern Desert of Egypt and the location of Um Halham (H) and Fawakhir (F) ophiolites (after Shackleton 1994). Inset displays the general map of Egypt and the location of figure is shown. *CED* Central Eastern Desert, *SED* Southern Eastern Desert

2001; El Bahariya and Arai 2003; Farahat et al. 2004; El-Gaby 2005; Abdel-Karim et al. 1996, 2008). In contrast, based on the mineral and bulk-rock data of the serpentinites a fore-arc setting was proposed (Stern 2004; Azer and Stern 2007; Abd El-Rahman et al. 2012; Azer et al. 2013; Abdel-Karim et al. 2015, 2016, 2017). To contribute toward solving this issue; we present bulk-rock and mineral compositional data for the metaultramafics of Um Halham and Fawakhir areas to better constrain their geochemical and geodynamic evolution.

Field characteristics

Um Halham

Um Halham area (Fig. 2) is situated between latitudes 26°19′48″–26°23′24″ N and longitudes 33°41′24″–33°48′36″ E in the western part of the CED and is covered mainly by volcano-sedimentary sequence thrusted to south over El-Rubshi ophiolites. The volcano-sedimentary sequence around Um Halham represents an interbedded sequence of clastic metasediments and metavolcanics. The western part

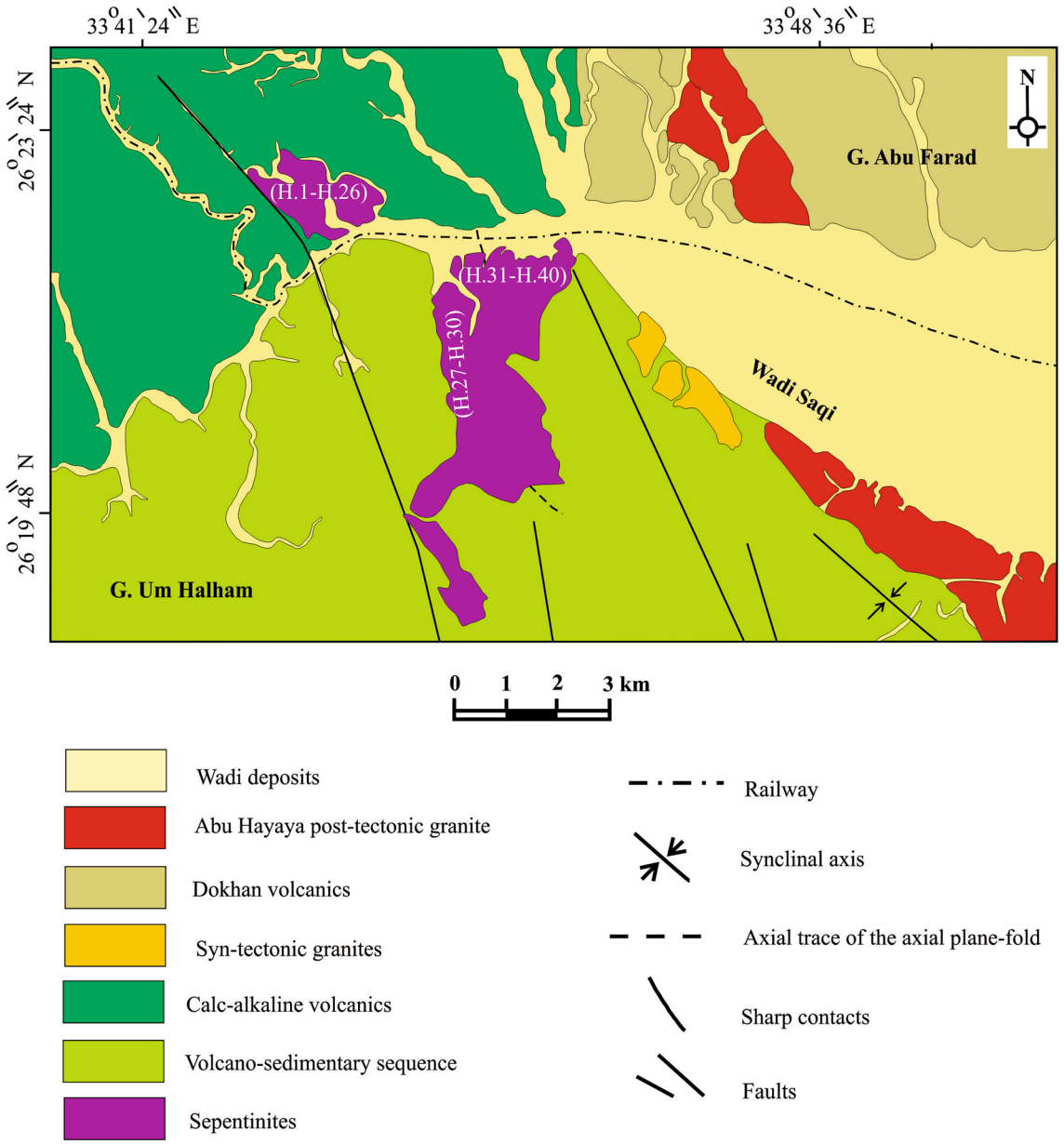

Fig. 2 Geologic map of Um Halham area (after Abu El-Ela 1990). Sample numbers are indicated

of the sequence starts at the base with clastic metasediments enclosing thin intercalations of iron ore bands, up to 10 cm thick, interbedded with metavolcanics (Abu El-Ela 1990). The eastern part of the sequence is represented mainly by pyroclasts and minor lava flows interbedded with metasediments. Um Halham ophiolites include talc–carbonates, serpentinites and chromitites. The area is intruded by small bodies of syn-tectonic granites and Abu Hayaya post-tectonic granites (Fig. 2). Serpentinite forms mountainous ridge with sharp irregular peaks (Fig. 3a). Talc–carbonates are thrusted over the volcano-sedimentary sequence (Fig. 3b). In some places, talc–carbonates exhibit conspicuous cavernous structure (Fig. 3c). Sometimes, chromite-rich serpentinites occur as fragments of variable sizes and shapes within talc–carbonates (Fig. 3d).

Fawakhir

Fawakhir area (Fig. 4) is located 93 km west of the Red Sea coast along Qift–Quseir asphaltic road between latitudes 25°57′36″–26°01′48″ N and longitudes 33°34′12″–33°40′12″ E. The total mapped area covers ~ 88 km^2. Fawakhir

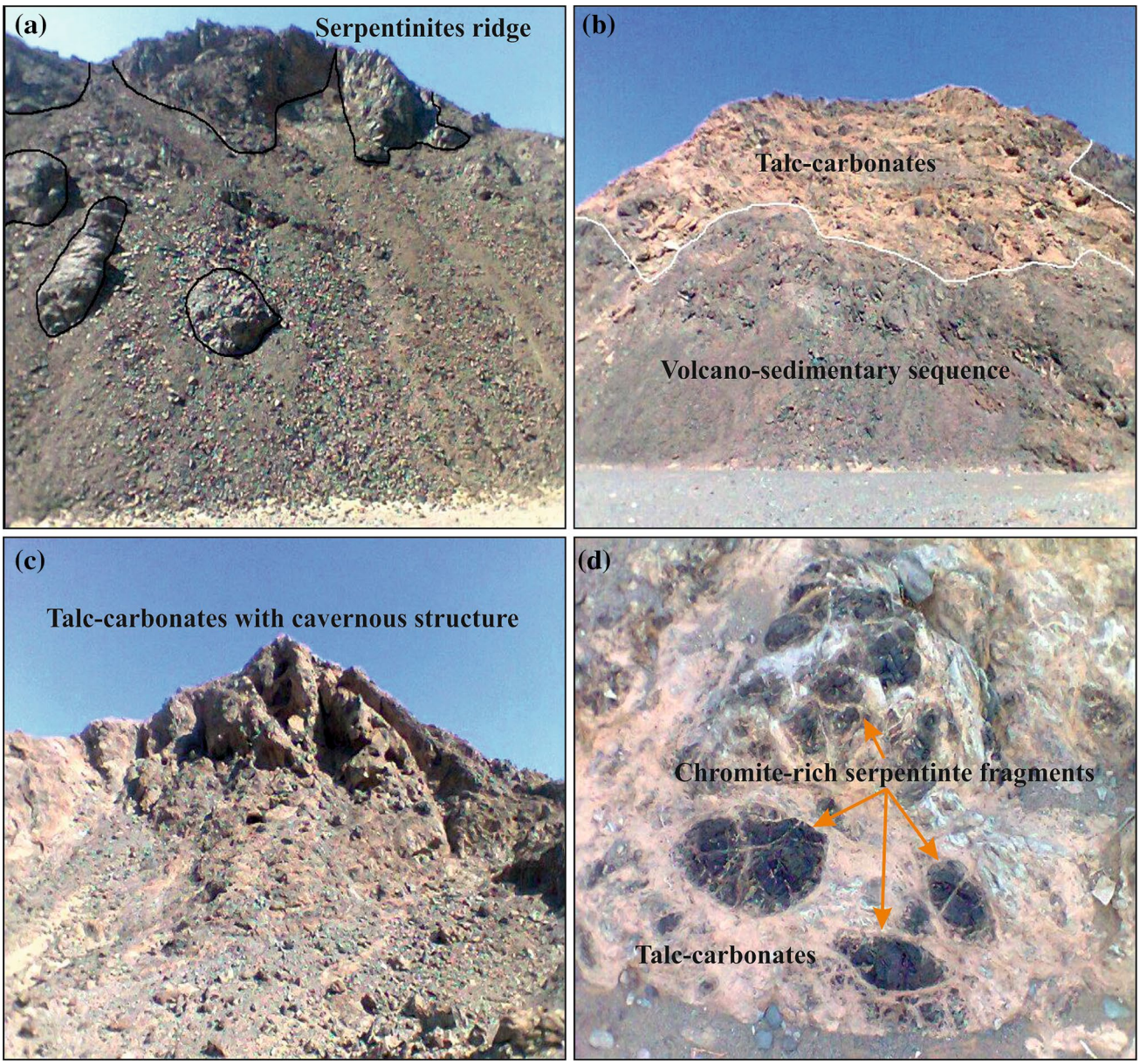

Fig. 3 Field photographs of Um Halham showing **a** serpentinites form mountainous-ridge with sharp irregular peaks; **b** talc–carbonates thrusted over volcano-sedimentary sequence; **c** talc–carbonates exhibit conspicuous cavernous structure; **d** chromite-rich serpentinite fragments in talc–carbonate rocks

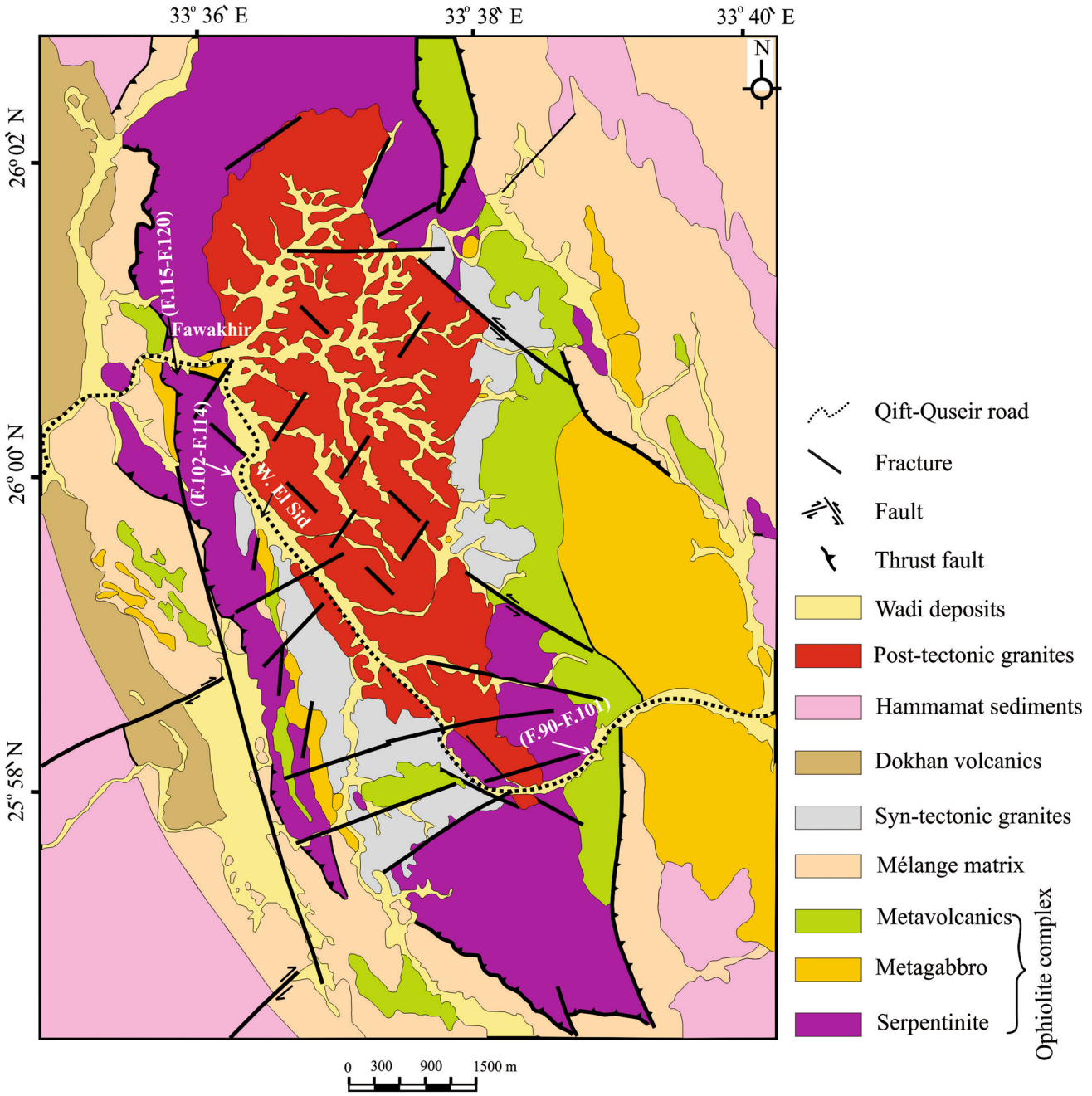

Fig. 4 Geologic map of Fawakhir area (after El-Sayed et al. 1999)

ophiolites situated between the Dokhan volcanics to the west and the Meatiq Dome ~ 15 km to the east. East dipping thrust zone characterized the western contact between the Fawakhir ophiolite suite and the Hammamat sediments, whereas its eastern contact with the Meatiq rocks is characterized by a zone of tectonic mélange, mylonitized rocks and highly-deformed 'flaser' gabbro. They contain mostly serpentinites, metagabbros, and metabasalts (El-Sayed et al. 1999). The Dokhan Volcanic rocks constitute a small mass located at the extreme western part of the study area. The serpentinites and metagabbros are intruded by Fawakhir post-tectonic granites with sharp contact (Fig. 5a). The serpentinites bordered Fawakhir granitoids from the west, north and south, however most of the eastern side lacks them (Fig. 4). Many shear zones cut across the serpentinized ultramafics which are altered to talc–carbonates along these shears (Abd El-Rahman et al. 2009a). Sometimes, the massive serpentinites show talc–carbonate alteration (Fig. 5b). The metaultramafics and adjacent rocks display sharp and distinct contacts. Serpentinites display sharp contact with

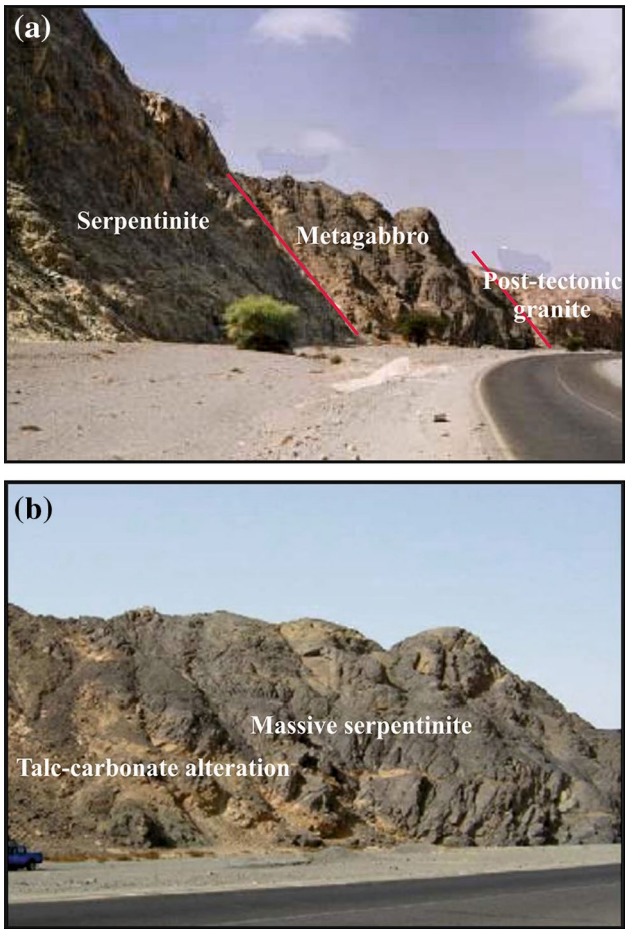

Fig. 5 Field photographs of Fawakhir area showing **a** sequence of serpentinite, metagabbro and post-tectonic granite along Qift–Quseir Road. Photo looking east; **b** massive serpentinite altered to talc–carbonate (buff color)

the underlying mélange. This sharp contact is characterized by a NNW–SSE trending deep thrust fault and a relatively narrow dark green schistose amphibolite band between the ultramafic and the mélange (Hassanen 1985). The adjacent country rocks lack the thermal metamorphic effect of the serpentinites indicating tectonic emplacement of the serpentinites (El-Sayed et al. 1999).

Petrography

The studied ophiolitic rocks are partially to completely serpentinized and comprise both massive and sheared varieties. Serpentinized peridotites and serpentinites belong to massive varieties while talc– and quartz–carbonates affiliated to sheared serpentinites. Both the Um Halham and Fawakhir metaultamafic rocks comprise serpentinized peridotites, serpentinites together with talc– and quartz–carbonates. They contain olivine, chromite and pyroxene relicts. Chromites are represented by homogenous and zoned crystals. The zoned chromites have darker cores compared to the outer rims which have lighter gray color and higher reflectance.

Serpentinized peridotites in Um Halham contain relicts of olivine (Fig. 6a) and clinopyroxene (Fig. 6b). Serpentine, tremolite–actinolite, chlorite and talc are the main metamorphic products. As metamorphism progresses, serpentinized peridotites change to serpentinites and carbonate–serpentinites. Serpentinites contain mainly serpentine minerals together with minor amounts of carbonates and opaques. Olivine relict and talc are recorded in few samples. Serpentinites show both pseudomorphic and interpenetrating textures. Serpentines formed after olivines exhibit mesh texture (Fig. 6c), whereas those developed after orthopyroxene display bastite texture (Fig. 6d). Sometimes, bastite texture accompanies schiller structure where magnetite grains outline original orthopyroxene cleavage planes (Fig. 6d). Carbonates exist as fine- to medium-grained patches substituting bastites or as veinlets substituting pre-existing chrysotile. Talc–carbonates consist principally of clusters or sparse patches of carbonates set in talc matrix, whereas quartz–carbonates essentially contain carbonates together with minor amounts of quartz. Chromites occur as zoned (Fig. 6e) and homogenous crystals with subordinate amounts of magnetites and sulfides.

Serpentinized peridotites in Fawakhir area consist of serpentine together with minor relics of olivine, chromite and pyroxene. Tremolite, talc, chlorite and iron oxides are secondary minerals. Serpentine minerals after olivine show pseudomorphic textures. The serpentinization affected olivine grain boundaries and fractures forming olivine mesh center (Fig. 6f). In the serpentinized peridotites pyroxene relicts present and sometimes replaced by talc (Fig. 6g). Serpentinites consist mainly of serpentine minerals associated with variable amounts of talc, carbonate and opaques. They exhibit pseudomorphic, interpenetrating (Fig. 6h) and hourglass textures (Fig. 6i). Talc–carbonates are fine-grained rocks with brownish yellow to reddish brown color. They contain essentially talc and carbonates with rare serpentine, chlorite and opaques. Talc occurs as vein-like and in the groundmass with clusters and patches of carbonate minerals. Zoned and homogenous chromites (Fig. 6j) occur with minor sulfides and magnetites.

Analytical techniques

A total of 46 mineral chemical analyses of olivine (12), clinopyroxene (12) and chromite (22) were performed using Phillips XL30 analyzer at the Central Laboratories of the Geological Survey in Cairo, Egypt. Operating conditions were 15 kv accelerating voltage, 20 nA beam current and 1 µm beam diameter. The raw data were corrected using ZAF correction factors. The analytical results (normalized

to 100%) of different minerals are given in Supplementary Table S.

Eighteen representative samples of Um Halham and Fawakhir were analyzed for major and trace elements. Major elements were analyzed using XRF techniques at the Institute of Geothermal Science, Noguchibaru, Beppu city, Japan. Fused beads were prepared from a mixture of specimen and $Li_2B_4O_7$ flux, diluted 1:5 at 950 °C to achieve accurate and precise results. Replicate analyses provided an overall procedural uncertainty better than 2% for major elements. The trace elements were analyzed after lithium metaborate/tetraborate fusion as well as nitric acid digestion of a 0.2-g sample using inductively coupled plasma–mass spectrometry techniques (ICP–MS) at the Acme Analytical Laboratories in Vancouver, BC Canada. The accuracy and reproducibility of this method lie within 2%. Bulk-rock geochemical analyses with detection limits are presented in Table 1.

Results

Mineral chemistry

Chromite chemical analyses are presented in Table S. Homogenous chromites and internal cores of zoned crystals are classified as Al–chromites while the outer rims have Cr–magnetite compositions (Fig. 7a). The fresh Al–chromite cores plot close to the Cr–Al join whereas the altered Cr–magnetite rims plot along Cr–Fe^{3+} join (Fig. 7a). Spinel in mantle peridotites is relatively unaffected by alteration and its Cr# particularly appears to remain unchanged during sub-solidus stage (Arai 1994). Geochemical consequences due to spinel alteration are discussed below. Al–chromites in the studied rocks have higher Cr# (> 60) akin to those of ophiolitic ultramafics of ANS including SED and CED (Fig. 7b, c) (Stern et al. 2004; Farahat et al. 2011; Ahmed et al. 2012; Abdel-Karim et al. 2016; Obeid et al. 2016). Their TiO_2 and Al_2O_3 contents are comparable to SSZ peridotites and overlap those of peridotites from Izu–Mariana and New Caledonia arcs (Fig. 7d; Kamenetsky et al. 2001).

Olivines range in composition from $Fo_{85.54–95.30}$ in Um Halham and from $Fo_{89.33–91.65}$ in Fawakhir and are like primary olivine relicts of ophiolitic metaultramafics from the ED of Egypt ($Fo_{89–96}$) (Table S) (Khudeir 1995; Khalil and Azer 2007; Khedr and Arai 2013; Obeid et al. 2016). These compositions correspond to chrysolite and forsterite. Moreover, their Fo-enriched nature is comparable to those observed in the ANS ophiolites and fore-arc peridotites further confirming their primary nature and suggest that the studied rocks are residual mantle after extensive melting (Stern et al. 2004). These inferences are also supported by spinels compositional data of the present study.

Clinopyroxenes have Mg# varying between 0.82 and 0.90 in Um Halham, and between 0.54 and 0.60 in Fawakhir. Their compositions rang from augite ($En_{47.94–65.38}Wo_{27.32–41.27}Fs_{6.46–10.53}Ac_{0.27–0.47}$) in Um Halham to pigeonite ($En_{44.92–48.35}Wo_{10.48–13.67}Fs_{39.42–43.01}Ac_{0.22–0.53}$) in Fawakhir (Table S) (Fig. 8a). Most of the clinopyroxenes in the serpentinized peridotites have Al_2O_3 (> 0.2 wt%) and Cr_2O_3 (> 0.4 wt%) contents higher than those observed in metamorphic clinopyroxenes reflecting magmatic origin (Nozaka 2010). The analyzed clinopyroxenes have low TiO_2 content characteristic of non-alkaline rocks (Le Bas 1962) and display a strong affinity to intra-oceanic fore-arc boninites (Fig. 8b). Their lower Na_2O and K_2O contents (≤ 0.15 and ≤ 0.04 wt%, respectively) indicate depleted nature of their host rocks. Moreover, the low Na_2O and TiO_2 suggest sub-oceanic source (Delavari et al. 2009).

Geochemistry

Bulk-rock chemistry of the studied rocks from Um Halham and Fawakhir is listed in Table 1. To diminish the effect of variable element dilution result from serpentinization process, major element oxides were recalculated on an anhydrous basis and plotted volatile-free. The rocks in both areas display different stages of metamorphism starting from the least affected serpentinized peridotites (LOI = 6.76–11.02) and then serpentinites (LOI = 12.46–26.78) to the most affected talc– and quartz–carbonates (LOI = 14.12–41.11). MgO is less affected by serpentinization and its higher content (MgO = 29.82–48.71 wt%) indicates more depleted mantle nature (Frey et al. 1985; Parkinson and Pearce 1998). The Mg# ranges from 0.85 to 0.94 in Um Halham and from 0.89 to 0.92 in Fawakhir, and are comparable to those from modern oceanic peridotites (Bonatti and Michael 1989) indicating also a limited adjustment of Mg and Fe. The depletion of Na_2O (< 0.05 wt%) and K_2O (~ 0.01 wt%) further confirms this implication (e.g., Abdel-Karim et al. 2016). Geochemical consequences due to alteration and metamorphism are also discussed below.

Al_2O_3 content seems to be relatively not influenced by serpentinization process demonstrating that the bulk-rock Al content typically reflects its original primary concentration (Bonatti and Michael 1989). The studied rocks have Al_2O_3 contents (0.15–3.52 wt%) overlap those from oceanic and active margin peridotites and fore-arc and Pan-African serpentinites (Floyd 1991; El Bahariya and Arai 2003; Abdel-Karim and Ahmed 2010). Their SiO_2/MgO ratios and Al_2O_3 contents are akin to ophiolitic peridotite (Bodinier and Godard 2003; Abdel-Karim et al. 2016) (Fig. 9a). Serpentinized peridotite of Um Halham (H.21) has higher Al_2O_3 (3.52 wt%) and CaO (8.18 wt%) compared to that of Fawakhir (F.98) (Al_2O_3 = 1.54 wt% and CaO = 0.9 wt%). Furthermore, serpentinites in both areas have low Al_2O_3 contents

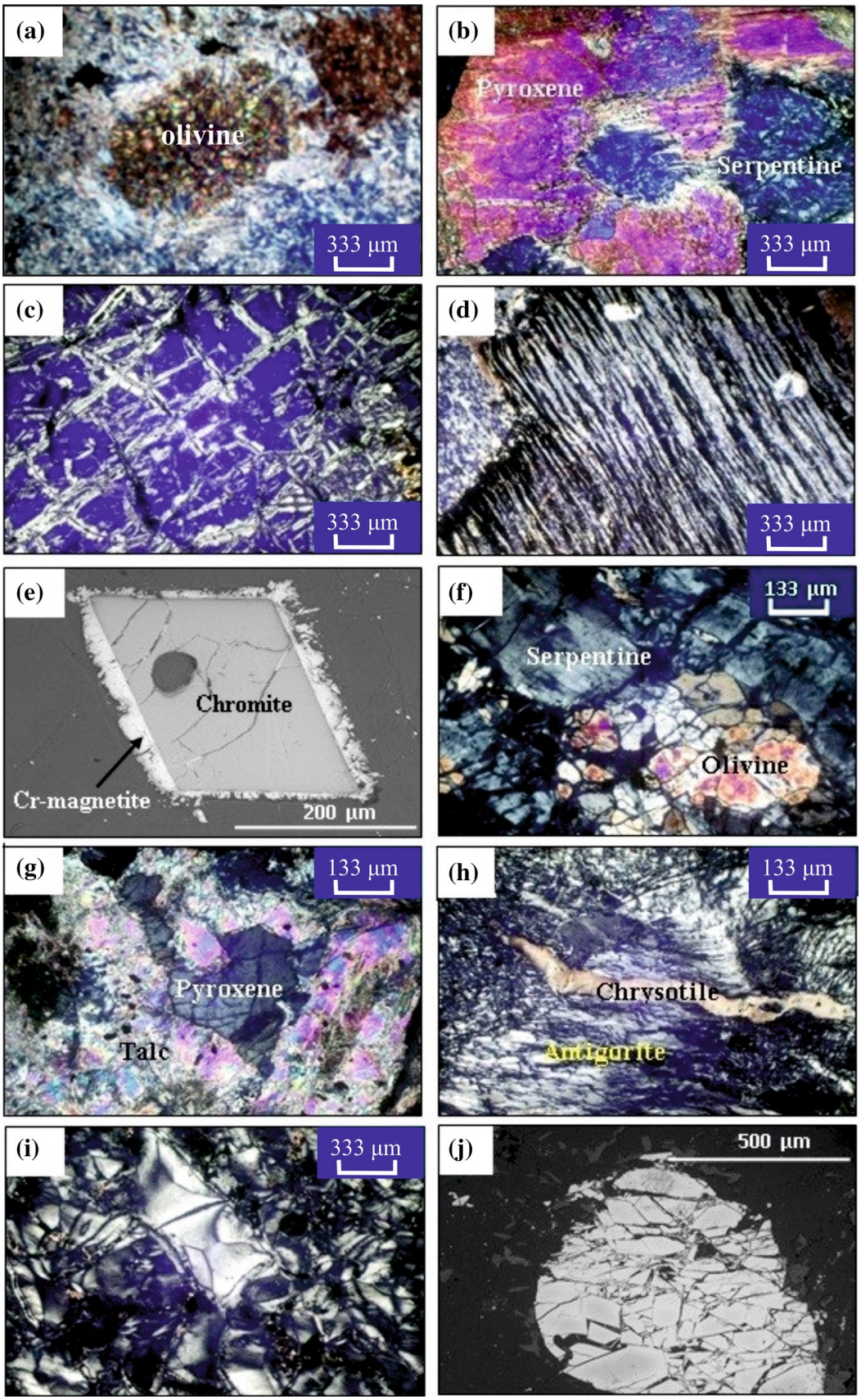
(a)
olivine
333 µm
(b)
Pyroxene
Serpentine
333 µm
(c)
333 µm
(d)
333 µm
(e)
Chromite
Cr-magnetite
200 µm
(f)
133 µm
Serpentine
Olivine
(g)
133 µm
Pyroxene
Talc
(h)
133 µm
Chrysotile
Antigorite
(i)
333 µm
(j)
500 µm

◂**Fig. 6** Photomicrographs taken under crossed nicols (e and j are back-scattered electron; BSE) displaying **a** fractured olivine crystal altered at margin to talc and serpentine minerals in serpentinized peridotite of Um Halham; **b** pyroxene crystal replaced by serpentine minerals in serpentinized peridotite of Um Halham; **c** mesh texture with isotropic mesh center in serpentinite of Um Halham; **d** bastite texture associated with schiller structure in serpentinite of Um Halham; **e** zoned chromite crystal mantled by Cr–magnetite with sharp contact in serpentinite of Um Halham; **f** mesh texture with olivine mesh center in serpentinized peridotite of Fawakhir; **g** talc and relics of pyroxene in serpentinized peridotite of Fawakhir; **h** chrysotile veinlet traversing antigorite matrix forming interpenetrating texture in serpentinite of Fawakhir **i** hourglass texture in serpentinite of Fawakhir; **j** fractured chromite crystal filled with serpentine minerals in serpentinite of Fawakhir

(0.15–0.86 wt%) and have a wide range of CaO (0.06–8.84 wt%). The low Al_2O_3 and CaO contents in most samples are comparable to fore-arc peridotites of ED (Zimmer et al. 1995; Azer and Khalil 2005; Azer and Stern 2007; Azer et al. 2013; Abdel-Karim et al. 2016). The Al_2O_3/SiO_2 and MgO/SiO_2 ratios are comparable to those of Arabian shield and fore-arc peridotites (Fig. 9b; Parkinson and Pearce 1998; Pearce et al. 2000; Ahmed and Habtoor 2015).

The studied rocks are enriched in compatible trace elements (Cr = 1338–3082 ppm, Ni = 557.6–2882.2 ppm and Co = 73.3–117.8 ppm) reflecting development from a depleted mantle peridotite source. Their trace element patterns (Fig. 10a) show fluid mobile element (FME; such as Cs, U, and Pb) enrichments resembling those of fore-arc serpentinites along with Sr enrichment which is not observed in serpentinized peridotite (Pearce et al. 2000; Song et al. 2009). These enrichments in FME, most likely point to the higher concentrations of these elements in the hydrating fluids of the mantle wedge. These hydrating fluids are rich in Cs, Pb, and Sr indicating that they were produced from sediment dehydration during shallow subduction (e.g., below fore-arcs; Deschamps et al. 2013 and references therein). Moreover, the high LILE contents [e.g., Ba/Th (up to 350), Ba/La (up to 70)] overlap those observed on mantle wedge serpentinites from diverse fore-arc systems suggesting interaction with sediment-derived fluids (Aziz et al. 2011; Kodolányi et al. 2012; Deschamps et al. 2013). Most of the trace elements (except Cs, U, Sr and Pb) are depleted compared to primitive mantle values (Fig. 10a; McDonough and Sun 1995) similar to mantle wedge serpentinites (Deschamps et al. 2013). Both the positive Pb-anomaly and the negative Nb-anomaly characterize the studied rocks (Fig. 10a). The overall low concentrations of trace element suggest high degrees of melt extraction of the mantle protolith, similar to mantle wedge serpentinites (Deschamps et al. 2013).

The REEs mobility during serpentinization process is insignificant, so they preserve the geochemical characteristics of the original mantle protolith (Deschamps et al. 2013). Bulk-rock REE contents of the studied rocks are relatively variable. Serpentinized peridotites have LREE composition ranging from ~2 to ~5 Chondrite and HREE from ~0.4 to ~2 Chondrite, whereas serpentinites have LREE composition ranging from ~1.5 to ~5 Chondrite and HREE from ~0.08 to ~0.3 Chondrite (Fig. 10b). Moreover, talc– and quartz–carbonates have LREE compositions varying from ~1.5 to ~4 Chondrite and HREE from ~0.2 to ~2 Chondrite (Fig. 10b). The studied rocks show no correlations between REEs and LOI confirming that the REE signatures of the mantle protolith were preserved during serpentinization and metamorphism (e.g., Savov et al. 2005a, b; Deschamps et al. 2013).

Serpentinized peridotite of Um Halham has both enriched LREE [$(La/Yb)_N = 2.1$] and HREE [$(Gd/Yb)_N = 1.03$] patterns as do quartz–carbonate [$(La/Yb)_N = 2.4$ and $(Gd/Yb)_N = 1.32$] (Fig. 10b). On the other hand, serpentinites and talc–carbonate rocks exhibit enriched LREE patterns with $(La/Yb)_N = 3.1–32.3$ and depleted HREE patterns with $(Gd/Yb)_N = 0.47–0.83$. Generally, serpentinites represent the most LREE-enriched rocks. Serpentinites, talc– and quartz–carbonates show variable positive Eu-anomaly compared with serpentinized peridotite (Fig. 10b).

Serpentinized peridotite of Fawakhir is LREE-enriched [$(La/Yb)_N = 16.74$] relative to HREE [$(Gd/Yb)_N = 2.21$] patterns (Fig. 10b). Moreover, serpentinites and quartz–carbonate have LREE patterns [$(La/Yb)_N = 3.6–14.35$] higher than HREE patterns [$(Gd/Yb)_N = 0.55–2.32$]. On the other hand, talc–carbonate (F.117) exhibits both LREE- and HREE-enriched patterns [$(La/Yb)_N = 11.5$ and $(Gd/Yb)_N = 17.5$]. In contrast to serpentinized peridotites, the analyzed samples from Fawakhir also display variable positive Eu-anomaly (Fig. 10b).

Discussion and conclusion

Geochemical consequences due to alteration and serpentinization

Generally, the ophiolitic ultramafics in the ED of Egypt are affected by low-grade green schist to medium-grade amphibolite facies metamorphism and altered to serpentinite and/or to combinations of serpentine, talc, chlorite, carbonates and magnetite (e.g., El-Sayed et al. 1999; Farahat 2008; Khedr and Arai 2013). Carbonate alteration affected the Egyptian ultramafic rocks but its timing and source remain controversial. It was attributed to mixing between CO_2-rich (mantle-derived) fluids and remobilized sedimentary carbonate (Stern and Gwinn 1990). Pure mantle (CO_2-bearing) source is also proposed based on stable isotope (i.e. O, C) (Boskabadi et al. 2017). Moreover, some magnesite veins in serpentinites from the ED were ascribed to an influx of

Table 1 Bulk-rock major (wt%), trace and rare-earth element (ppm) data of the studied metaultramafics

Area	Um Halham										Fawakhir								Detection limit
Rock type	Serpentinized peridotite	Serpentinite						Talc–carbonate		Quartz–carbonate	Serpentinized peridotite	Serpentinite					Talc–carbonate	Quartz–carbonate	
Sample no.	H.21	H.27	H.29	H.33	H.19	H.28	H.36	H.37	H.26	H.15	F.98	F.114	F.96	F.112	F.99	F.100	F.117	F.94	
SiO_2	46.38	45.22	45.49	46.2	44.81	43.79	46.08	45.02	51.47	10.28	46.96	43.05	38.96	42.27	45.66	44.8	39.9	41.58	0.02%
TiO_2	0.08	0.03	0.01	0	0.02	0.01	0	0.01	0.01	0.04	0.04	0.02	0.01	0.01	0.01	0.01	0.02	0.01	0.01%
Al_2O_3	3.52	0.51	0.47	0.37	0.28	0.35	0.15	0.16	0.17	1.87	1.54	0.17	0.21	0.15	0.86	0.6	0.26	0.2	0.03%
Fe_2O_3	10.43	10.45	7.75	7.62	7.43	7.82	6.53	8.46	6.4	6.35	8.31	10.68	10.32	9.03	7.76	8.78	10.92	7.9	0.04%
MnO	0.17	0.13	0.07	0.08	0.12	0.1	0.06	0.16	0.04	0.66	0.07	0.14	0.29	0.14	0.07	0.06	0.16	0.15	0.01%
MgO	29.82	39.26	43.59	46	44.79	37.45	47.67	39.71	39.62	32.15	40.77	42.27	44.06	42.68	43.37	43.84	46.96	48.71	0.01%
CaO	8.18	3.54	0.56	0.09	1.14	8.84	0.06	5.9	1.48	47.96	0.9	3.03	4.63	4.21	0.6	0.43	0.56	0.53	0.01%
Na_2O	0.2	0	0.03	0	0.03	0.01	0	0.01	0.09	0	0.03	0.03	0.03	0.05	0.03	0.04	0.02	0.02	0.01%
K_2O	0.01	0	0	0	0	0	0	0	0	0	0	0	0	0	0	0	0	0	0.01%
P_2O_5	0	0	0	0	0	0	0	0	0	0.01	0	0	0	0	0	0	0	0	0.01%
Total	98.79	99.14	97.97	100.36	98.62	98.37	100.55	99.43	99.28	99.32	98.62	99.39	98.51	98.54	98.36	98.56	98.8	99.1	
LOI	6.76	12.66	12.67	13.31	13.87	15.82	17.72	26	23.4	41.11	11.02	26.78	19.56	15.55	12.6	12.46	14.12	33.31	
Mg #	0.85	0.88	0.92	0.92	0.92	0.90	0.94	0.90	0.92	0.91	0.91	0.89	0.89	0.90	0.92	0.91	0.89	0.92	
Cr	2298	3335	2458	2326	2588	2305	2121	2290	3082	117	2489	2808	1338	1501	2132	2125	1841	1944	1 ppm
Ni	557.6	1314.9	2598.4	1231.1	2446.6	2287.7	1390.2	2473.3	1995.7	111.5	1997	2703.1	1890.1	2882.3	2340.7	2424.6	937.9	1959	1 ppm
Co	92	117.8	86	90.3	107	95.4	86.9	77	77.7	10.4	86	98.9	81.9	100.8	83.2	93.2	98.7	73.3	0.5 ppm
Pb	0.3	0.3	0.2	0.5	0.2	0.5	0.5	0.7	0.2	1.2	0.2	0.2	0.2	0.6	0.1	0.1	0.4	2	0.1 ppm
Sr	13.1	27.1	10.2	0.8	16.3	14.8	10.3	5.6	11.3	106.8	6.9	70.1	76	44.5	9.2	8.1	9.6	254.6	0.5 ppm
Ba	16	11	8	0.5	18	25	5	5	2	13	4	10	35	3	3	4	3	11	0.5 ppm
Rb	0.7	0.1	0.1	0.08	0.5	0.2	0.07	0.04	0.1	0.05	0.5	0.02	0.05	0.04	0.07	0.09	0.09	0.06	0.01 ppm
Cs	0.2	0.05	0.05	0.05	0.05	0.05	0.05	0.05	0.05	0.05	0.05	0.05	0.05	0.05	0.05	0.05	0.05	0.05	0.02 ppm
Zr	4.1	1	0.5	0.2	1	0.3	0.3	0.9	0.4	2.9	2.2	0.3	0.5	0.05	0.3	0.2	0.8	0.3	0.1 ppm
Nb	0.05	0.05	0.05	0.05	0.05	0.05	0.8	0.05	0.05	0.05	0.05	0.05	0.05	0.05	0.05	0.05	0.05	0.05	0.01 ppm
Hf	0.1	0.05	0.05	0.05	0.05	0.05	0.05	0.05	0.05	0.05	0.05	0.05	0.05	0.05	0.05	0.05	0.05	0.05	0.01 ppm
Th	0.1	0.1	0.1	0.1	0.1	0.1	0.1	0.1	0.1	0.1	0.3	0.1	0.1	0.1	0.1	0.1	0.1	0.1	0.1 ppm
U	0.05	0.05	0.05	0.05	0.05	0.2	0.05	0.05	0.05	0.05	0.05	0.05	0.1	0.05	0.05	0.05	0.05	0.05	0.01 ppm
Ta	0.05	0.05	0.05	0.05	0.05	0.05	0.05	0.05	0.2	0.05	0.05	0.05	0.05	0.05	0.05	0.05	0.05	0.05	0.01 ppm
Y	1.7	0.3	0.05	0.07	0.1	0.1	0.05	0.05	0.03	3.3	0.7	0.05	0.5	0.05	0.05	0.08	0.05	1	0.02 ppm
La	0.7	0.3	0.5	0.5	0.9	0.7	0.4	0.3	0.4	0.9	1.4	0.4	0.5	0.3	1.2	0.4	0.4	0.8	0.2 ppm
Ce	0.8	0.3	0.1	0.2	0.1	0.2	0.2	0.1	0.05	1.2	2.5	0.4	0.5	0.1	0.3	0.1	0.2	0.6	0.1 ppm
Pr	0.1	0.04	0.012	0.017	0.02	0.01	0.02	0.014	0.012	0.17	0.29	0.03	0.1	0.01	0.012	0.014	0.01	0.08	0.01 ppm

Table 1 (continued)

Area	Um Halham									Fawakhir								Detection limit
Rock type	Serpentinized peridotite	Serpentinite					Talc–carbonate		Quartz–carbonate	Serpentinized peridotite	Serpentinite					Talc–carbonate	Quartz–carbonate	
Sample no.	H.21	H.27	H.29	H.33	H.19	H.28	H.36	H.37	H.26	H.15	F.98	F.114	F.96	F.112	F.99	F.100	F.117	F.94	
Nd	0.6	0.25	0.15	0.2	0.1	0.15	0.2	0.2	0.15	1	1.1	0.15	0.2	0.1	0.1	0.2	0.15	0.4	0.1 ppm
Sm	0.15	0.04	0.02	0.03	0.02	0.03	0.04	0.03	0.03	0.32	0.16	0.03	0.04	0.02	0.03	0.04	0.025	0.11	0.01 ppm
Eu	0.06	0.06	0.011	0.016	0.013	0.015	0.018	0.017	0.013	0.19	0.03	0.03	0.01	0.02	0.013	0.017	0.03	0.06	0.01 ppm
Gd	0.3	0.04	0.02	0.03	0.02	0.03	0.04	0.04	0.03	0.43	0.16	0.04	0.07	0.03	0.02	0.03	0.53	0.15	0.01 ppm
Tb	0.05	0.08	0.02	0.05	0.03	0.06	0.08	0.05	0.04	0.08	0.02	0.05	0.01	0.02	0.03	0.07	0.05	0.03	0.01 ppm
Dy	0.37	0.08	0.03	0.04	0.02	0.03	0.04	0.03	0.02	0.55	0.15	0.04	0.07	0.03	0.24	0.04	0.05	0.19	0.01 ppm
Ho	0.09	0.018	0.012	0.014	0.012	0.016	0.018	0.016	0.014	0.11	0.02	0.015	0.018	0.012	0.014	0.016	0.01	0.02	0.01 ppm
Er	0.23	0.04	0.01	0.02	0.05	0.01	0.02	0.02	0.01	0.33	0.07	0.015	0.07	0.015	0.015	0.018	0.03	0.1	0.01 ppm
Tm	0.04	0.09	0.03	0.05	0.02	0.04	0.07	0.05	0.03	0.04	0.01	0.05	0.05	0.05	0.02	0.05	0.05	0.02	0.01 ppm
Yb	0.24	0.07	0.02	0.03	0.02	0.03	0.04	0.04	0.03	0.27	0.06	0.025	0.025	0.025	0.03	0.04	0.025	0.16	0.01 ppm
Lu	0.04	0.08	0.02	0.05	0.05	0.06	0.08	0.07	0.05	0.04	0.01	0.04	0.05	0.03	0.05	0.08	0.05	0.02	0.01 ppm

mantle and metamorphic-degassing of CO_2 (e.g., Ghoneim et al. 2003; Hamdy and Lebda 2007).

Despite the mineralogical modifications in peridotites during serpentinization processes, geochemical studies of serpentinites show insignificant changes in major elements (except for Ca) at the hand-specimen scale (e.g., Mével 2003; Deschamps et al. 2010, 2013). However, except for two samples (H.21 and H.28), the low CaO contents (0.06–4.63 wt%) in the serpentinized peridotite and serpentinites reflect limited effect of Ca–metasomatism which is further supported by the absence of appreciated correlation between CaO and LOI in all samples. Moreover, bulk-rock data of serpentinized peridotites similarly indicate insignificant modifications occur in the trace element compositions (excluding U or Sr) during serpentinization (e.g., Niu 2004; Paulick et al. 2006; Deschamps et al. 2013). Consequently, major and trace element compositions can be used to define the nature of the serpentinites protolith in subduction zones (Chalot-Prat et al. 2003; Hattori and Guillot 2007; Deschamps et al. 2013).

Low-temperature serpentinization process leads to initial growth of slightly Fe-enriched chromite because of fluid infiltration along chromite cracks and grain boundaries (Barnes 2000). At higher temperature, further fluid access and reaction give rise to extensive magnetite replacement of chromite (Barnes 2000). Chromite alteration caused by serpentinization process in the late stage of magmatism and possibly accompanying emplacement of the ophiolite complex (e.g., Khudeir et al. 1992; Khalil and Azer 2007). The altered Cr–magnetite rims have higher total iron and lower Cr_2O_3, Al_2O_3, MgO and Cr# than the fresh Al–chromite cores (Table S) indicating an alteration event. Moreover, the Cr–magnetite plot on the Cr–Fe^{3+} joins close to Fe^{3+} apex (Fig. 7a) reflecting Fe_2O_3 increase and loss in Cr_2O_3 and Al_2O_3 during alteration. Their high Fe^{3+} reflects oxidation conditions during alteration (Anzil et al. 2012).

Metamorphic grade

Chromite cores continually equilibrated with magnetite rims document metamorphic grade conditions (Barnes 2000). The relative proportions of the trivalent ions (i.e. Cr^{3+}, Al^{3+} and Fe^{3+}) of chromite are unaffected by metamorphism up to lower temperature amphibolite facies implying restricted mobility of these elements occurred under lower amphibolite (Barnes 2000). Therefore, chromite in lower temperature amphibolite facies preserves its primary igneous chemistry and can be used to estimate the metamorphic grade (Barnes 2000). According to Fig. 11, almost all the Al–chromite cores are equilibrated at temperature below ~ 500–550 °C corresponding to lowest amphibolite facies metamorphism (Sack and Ghiorso 1991; Barnes 2000). So, they reflect magmatic composition not influenced by metamorphism (e.g.,

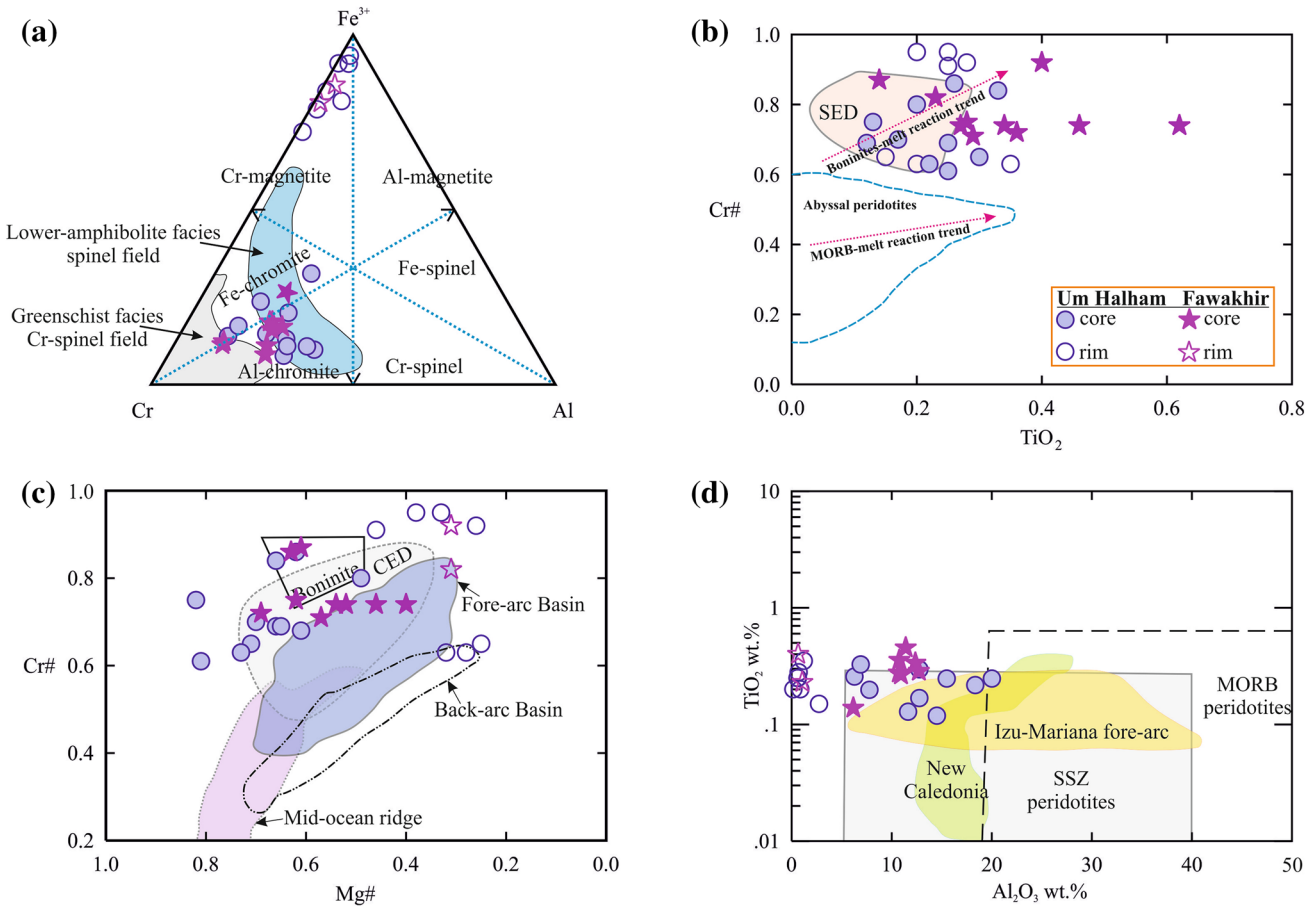

Fig. 7 Plot of chromites on **a** Cr–Fe^{3+}–Al ternary diagram. Greenschist and lower-amphibolite metamorphic facies compositional fields are after Evans and Frost (1975) and Suita and Strieder (1996); **b** Cr# versus TiO_2. The abyssal peridotites compositional field and trends of the effect of MORB–melt reaction on refractory abyssal peridotite spinels and of boninite–melt reaction on refractory SSZ peridotite spinels are from Choi et al. (2008); **c** Cr# versus Mg# diagram exhibit fields of different tectonic setting (Dick and Bullen 1984; Bloomer et al. 1995; Ohara et al. 2002; Stern et al. 2004). Chromite compositional fields of SED (Ahmed et al. 2012) and CED (Farahat et al. 2011) serpentinites are also shown; **d** Al_2O_3–Ti_2O. Spinels compositional fields of SSZ and MORB-type peridotites as well as those of fore-arc peridotites from the Izu–Mariana and New Caledonia are after Kamenetsky et al. (2001)

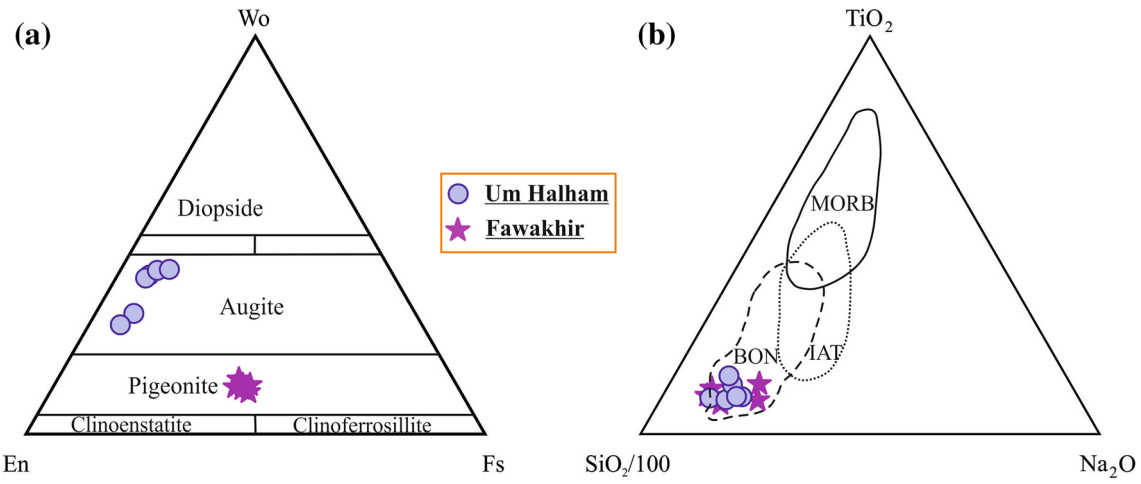

Fig. 8 Plot of the analyzed pyroxenes on **a** En–Wo–Fs ternary diagram (after Morimoto et al. 1988); **b** SiO_2–TiO_2–Na_2O ternary diagram (after Beccaluva et al. 1989)

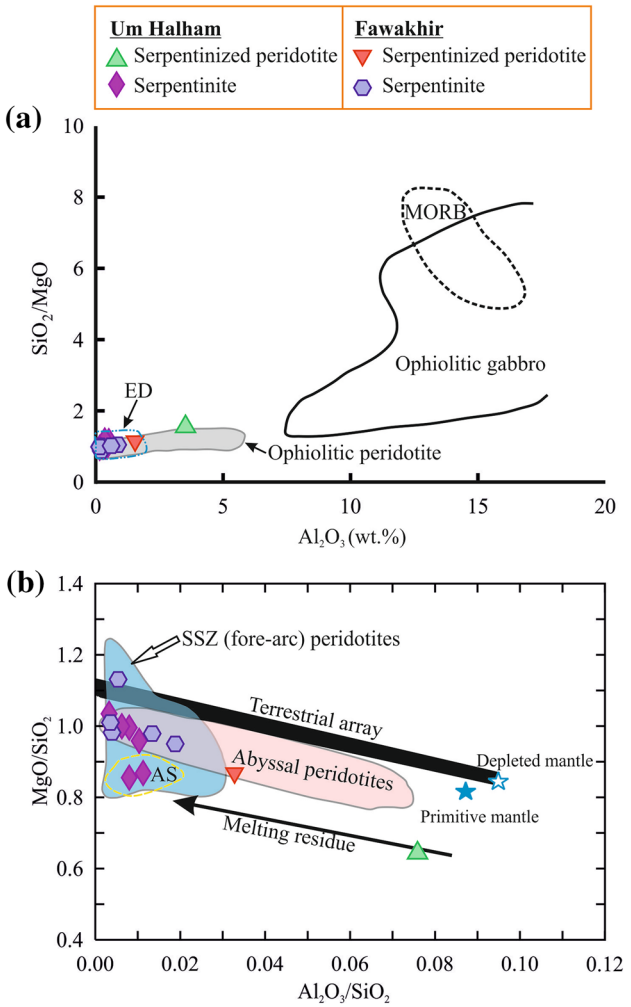

Fig. 9 **a** Bulk-rock Al_2O_3 versus SiO_2/MgO ratio diagram. Fields of ophiolitic peridotite, ophiolitic gabbro and MORB are from Bodinier and Godard (2003). ED field is ophiolitic peridotite compositions from both the Central and Southern Eastern Desert of Egypt (after Azer and Khalil 2005; Azer and Stern 2007; Azer et al. 2013; Abdel-Karim et al. 2016); **b** MgO/SiO_2 versus Al_2O_3/SiO_2 diagram. Primitive and depleted mantle values are from McDonough and Sun (1995) and Salters and Stracke (2004), respectively. The "terrestrial array" represents the bulk silicate Earth evolution (Jagoutz et al. 1979; Hart and Zindler 1986). Fields of abyssal and fore-arc peridotite are from Niu (2004), Pearce et al. (2000) and Parkinson and Pearce (1998). AS represents the field of Arabian Shield ophiolitic peridotite (Ahmed and Habtoor 2015)

Barnes 2000). On the other hand, altered chromite rims have nearly pure magnetite compositions with restricted Cr-solubility indicating magnetite development at < 500 °C (Fig. 11; Sack and Ghiorso 1991; Barnes 2000).

Indeed, this inference is confirmed by plotting the analyzed Al–chromite cores in the primary spinel fields of greenschist and lower-amphibolite metamorphic facies (Fig. 7a: Evans and Frost 1975; Suita and Strieder 1996). Thus, the studied rocks experienced metamorphism grade from greenschist up to lower-amphibolite metamorphic facies (Figs. 7a, 11).

Modification of the mantle source by subducted components

The studied rocks exhibit very low Nb, Ta, Zr and Hf concentrations along with sub-chondritic ratios of Nb/Ta (0.3–16) and Zr/Hf (mostly 1–20) indicating depletion of their mantle source by earlier melting extraction event (e.g., Yang and Zhou 2009).

Mantle source modification by continental materials and/or subduction-related slab melts/fluids has been confirmed for ophiolitic utramafics (e.g., Sharma and Wasserburg 1996; Gruau et al. 1998; Delavari et al. 2009; Ahmed et al. 2012; Abdel-Karim et al. 2016). Ahmed et al. (2012) which suggested that Gebel Mudarjaj ultramafics were formed by contamination of arc-related magmas by lower crustal gabbroic rocks. Recently, Abdel-Karim et al. (2016) indicated that the Gerf serpentinites could have been generated by contamination of their mantle source with crustal material and/or subduction-related slab fluids.

On the $(La/Sm)_N$ versus $(1/Sm)_N$ diagram of Sharma and Wasserburg (1996) (Fig. 12), a comparison presented between the studied metaultramafics and model peridotites produced from contaminated residual harzburgites with MORB melts or continental crust components. The studied rocks display LREE-enrichment [$(La/Sm)_N$ average 10; Fig. 12]. Moreover, they plot around lines demonstrating mantle modified with crustal materials and/or subduction-related slab melts/fluids (Fig. 12; Gruau et al. 1998). However, their low Th/Nb ratios (mostly 0.1–2) and negative Zr anomalies argue against significant crustal contamination (e.g., Yang and Zhou 2009). Thus, their high $(La/Sm)_N$ resulted from subduction-related slab melts/fluids influx during the evolution of the mantle in a subduction zone setting. The low Ce/Pb (average 1.6) and high Ba/Nb (average 191) together with the negative Nb anomalies further support the input of subduction-related slab melts/fluids into their mantle source. The origin of the LREE-enriched Trinity ophiolite (Fig. 12) has also been attributed to contamination of their mantle source (mantle restite) with crustal components (Gruau et al. 1998). This contamination could occur during evolution of the mantle in SSZ setting or following ophiolite complex obduction on the continental crust (Gruau et al. 1998; Delavari et al. 2009). The trend of increasing $(La/Sm)_N$ indicates variable input of subduction-related slab melts/fluids into the mantle source of the ED ophiolites (Fig. 12).

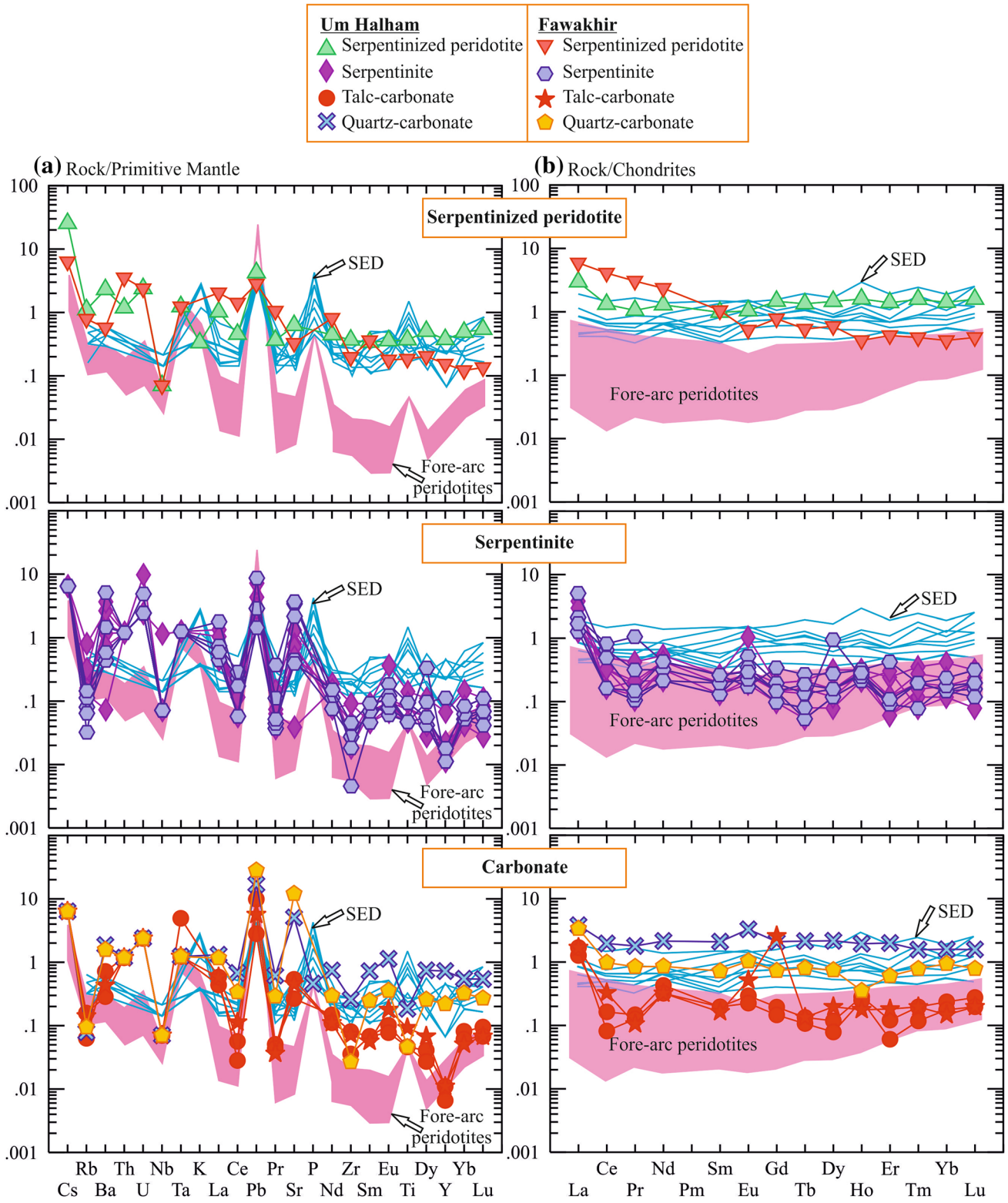

Fig. 10 **a** Primitive mantle-normalized trace element patterns; **b** chondrite-normalized REE patterns. Normalization values are after McDonough and Sun (1995). Data sources: fore-arc peridotites (Pearce et al. 2000; Song et al. 2009); SED ophiolitic ultramafics (Abdel-Karim et al. 2016)

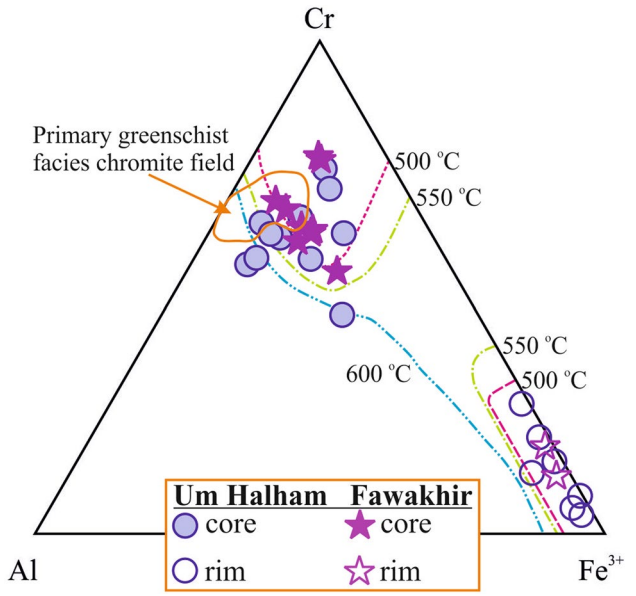

Fig. 11 Spinel data from the studied rocks compared with Sack and Ghiorso spinel stability fields for chromite and magnetite (after Barnes 2000)

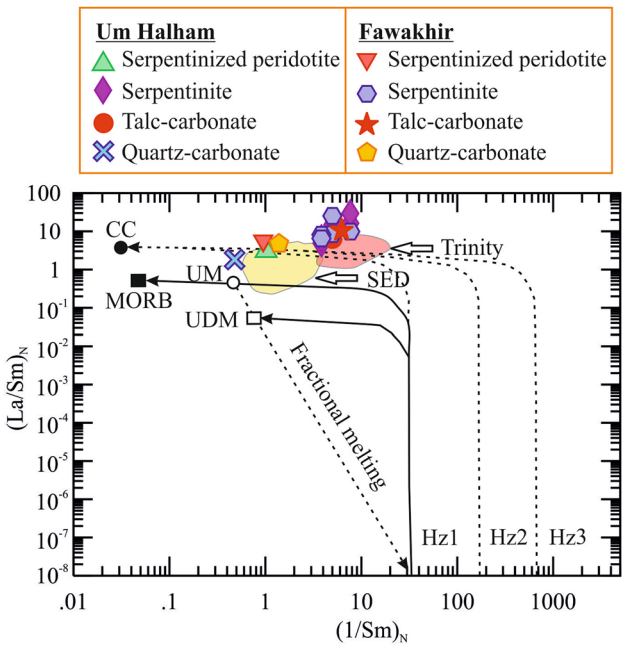

Fig. 12 Sharma and Wasserburg (1996) diagram showing chondrite-normalized $(La/Sm)_N$ versus $(1/Sm)_N$. *MORB* mid-ocean ridge basalts, *UM* upper mantle composition, *UDM* ultra-depleted melt composition, *CC* continental crust composition, *HZ1, HZ2 and HZ3* model harzburgite compositions. Fields of SED and Trinity ophiolite are shown for comparison (Gruau et al. 1998; Abdel-Karim et al. 2016)

Protolith geochemical fingerprints

Several studies have shown insignificant mobility of major elements and protolith geochemical fingerprints were preserved during serpentinization process (e.g., O'Hanley 1996; Mével 2003; Niu 2004; Deschamps et al. 2013).

The low CaO contents in serpentinized peridotite and serpentinites are comparable to values noticed on ophiolitic peridotites (Bodinier and Godard 2003), whereas the two samples (H.21 and H.28) with high CaO contents are like serpentinized lherzolites (Deschamps et al. 2013). Moreover, the low Al_2O_3/SiO_2 ratios (mostly < 0.03) of serpentinized peridotite and serpentinites akin to fore-arc mantle wedge serpentinites and indicate that their protoliths had underwent partial melting before serpentinization process which has no influence on this ratio (e.g., Snow and Dick 1995; Paulick et al. 2006; Deschamps et al. 2013). Also, their low MgO/SiO_2 ratios (< 1.1) resemble serpentinized lherzolite and harzburgite (Deschamps et al. 2013). They have low TiO_2 contents (0.0–0.08 wt%) compared to depleted mantle composition but like subduction zone serpentinites (Salters and Stracke 2004; Deschamps et al. 2013).

Trace element compositions (principally REEs) of serpentinized mantle rocks can be used to interpret the nature of the mantle protolith and the interactions with fluid/melt (Deschamps et al. 2013). The low HFSE content reveals high degrees of melt extraction (e.g., Parkinson and Pearce 1998). Positive Pb-anomaly present on spider-diagrams may reflect a protolith nature or fluid percolation during serpentinization (Fig. 10a) (Godard et al. 2008; Deschamps et al. 2013).

Magma nature

The low Al_2O_3 content in the studied rocks is consistent with a depleted upper mantle source (Bonatti and Michael 1989). They display higher Mg# numbers together with Cr and Ni enrichment reflecting development from a depleted mantle peridotite source (e.g., Khalil 2007; Abdel-Karim et al. 2016). Their high bulk-rock MgO and SiO_2 and low Al_2O_3 and TiO_2, together with clinopyroxenes data suggest boninitic and fore-arc affinity. They have Al–chromites with higher Cr# indicating that they represent highly depleted mantle residues after higher degrees of melting. The degrees of melting were estimated based on fresh chromite chemistry using the empirical equation of Hellebrand et al. (2001) [i.e. Melting degree (F %) = 10*ln (Cr#) + 24]. According to this equation, the degrees of melting vary between 19 and 24% similar to that of Gebel Mudarjaj in the SED of Egypt (Ahmed et al. 2012) and are totally within the range (15–40%) of SSZ peridotites (Pearce et al. 2000; Mellini et al. 2005).

On the TiO_2–Cr# diagram (Fig. 7b), the analyzed spinels plot around the boninite–melt reaction trend which is completely different from the MORB–melt trend of the abyssal peridotites. Moreover, the Al–chromites have Cr# and TiO_2 compositional features typical of primary

spinels from fore-arc depleted mantle peridotites with boninitic characteristics (Dick and Bullen 1984; Arai 1992) (Fig. 7b). The high Cr# (> 60) and Mg# (49–82) of Al–chromite cores are also comparable to those from mantle-derived peridotites which support the primary nature and boninitic affiliation (Fig. 7c) (Roeder 1994; Mondal et al. 2001). Furthermore, the clinopyroxene compositions correspond to that from boninites (Fig. 8b).

Tectonic implications

Serpentinized peridotite and serpentinites have low MgO/SiO_2 ratios (< 1.1) according with SSZ peridotites from fore-arc setting (Fig. 9b; Parkinson and Pearce 1998; Pearce et al. 2000). Generally, the studied rocks are depleted in Al_2O_3 content indicating a SSZ setting (Bonatti and Michael 1989). The negative Nb-anomaly is consistent with SSZ geochemical fingerprints and is typical of fore-arc peridotites (Fig. 10a) (Hawkins 2003; Song et al. 2009). Furthermore, the characteristic positive Pb-anomaly displayed on spider-diagrams is similar to fore-arc peridotites (Fig. 10a) (Hawkins 2003; Deschamps et al. 2013).

Fresh chromite core composition is a good proxy to define the tectonic setting of ultramafic mantle rocks (Dick and Bullen 1984; Arai 1992). The low contents of Al_2O_3 and TiO_2 in the analyzed Al–chromites are identical to peridotites from SSZ setting (Fig. 7d). There is some overlap with the spinels compositional range from the Izu–Mariana fore-arc and New Caledonia mantle peridotites (Fig. 7d). Subduction-related mantle rocks including mantle wedge and fore-arc rocks have spinels with elevated Cr# (> 0.40) (Dick and Bullen 1984; Ozawa 1994; Parkinson and Arculus 1999) which is the case of the studied rocks. The high Cr# (> 60) of the analyzed Al–chromites is comparable to those of modern fore-arc peridotites but clearly higher than spinels from MOR and back-arc peridotites (Fig. 7c; Ahmed et al. 2001; Stern et al. 2004; Farahat et al. 2011; Abdel-Karim et al. 2016). Moreover, the high Cr# is also similar to that observed in the chromitites of boninitic affinity existed in the deeper portion of the mantle section (Rollinson and Adetunji 2015). The Cr# and Mg# relationship shows that the studied rocks are similar to depleted fore-arc peridotites (Fig. 7c) (Ishii et al. 1992; Parkinson and Pearce 1998). Furthermore, they are similar to fore-arc serpentinites from Mariana in the western Pacific and Tso Morari in the NW Himalaya (Ishii et al. 1992; Guillot et al. 2001).

Acknowledgements Many thanks to H.M. Helmy who kindly carried out the XRF analyses of the Major elements during his stay in Japan. Critical comments and constructive reviews by M.K. Azer and an anonymous referee and by editor, Wolf-Christian Dullo, substantially improved an early version of this manuscript.

References

Abd El-Rahman Y, Polat A, Dilek Y, Fryer BJ, El-Sharkawy M, Sakran S (2009a) Geochemistry and tectonic evolution of the Neoproterozoic incipient arc–forearc crust in the Fawakhir area, Central Eastern Desert, Egypt. Precambr Res 175:116–134

Abd El-Rahman Y, Polat A, Dilek Y, Fryer BJ, El-Sharkawy M, Sakran S (2009b) Geochemistry and tectonic evolution of the Neoproterozoic Wadi Ghadir ophiolite, Eastern Desert. Egypt Lithos 113:158–178

Abd El-Rahman Y, Ploat A, Dilek Y, Kusky T, El-Sharkawy M, Said A (2012) Cryogenian ophiolite tectonics and metallogeny of the Central Eastern Desert of Egypt. Int Geol Rev 54(16):1870–1884

Abd El-Salam MG, Stern RJ (1996) Sutures and shear zones in the Arabian-Nubian Shield. J Afr Earth Sci 23:289–310

Abdel-Karim AM, Ahmed Z (2010) Possible origin of the ophiolites of Eastern Desert of Egypt, from geochemical prospectives. Arab J Sci Eng 34:1–27

Abdel-Karim AM, El-Mahallawi MM, Finger F (1996) The ophiolite mélange of Wadi Dunqash and Wadi Arayis, Eastern Desert of Egypt: petrogenesis and tectonic evolution. Acta Mineral Petrogr 37:129–141

Abdel-Karim AM, Azzaz SA, Moharem AF, El-Alfy H (2008) Petrological and geochemical studies on the ophiolite and island arc association of Wadi Hammaryia, Egypt. Arab J Sci Eng 33(1C):117–138

Abdel-Karim AM, Ali S, Helmy HM, El-Shafei SA (2015) Mantle rocks from Neoproterozoic Gerf ophiolite, South Eastern Desert, Egypt: a case for a possible boninitic fore-arc oceanic fragment. The second International Conference on New Horizons in Basic and Applied Science, 1–6 August 2015, Hurghada, Egypt

Abdel-Karim AM, Ali S, Helmy HM, El-Shafei SA (2016) Fore-arc setting of the Gerf ophiolite, Eastern Desert, Egypt: evidence from mineral chemistry and geochemistry of ultramafites. Lithos 263:52–65

Abdel-Karim AM, Ali S, El-Shafei SA (2017) Mineral chemistry and geochemistry of ophiolitic ultramafics from central Eastern Desert, Egypt: a case for contaminated mantle-derived magma. Geophysical Research Abstracts Vol. 19, EGU2017-16680-1, EGU General Assembly 2017

Abu El-Ela FF (1990) Bimodel volcanism of volcanosedimentary sequence around Gabal Um Halham, central Eastern Desert, Egypt. Bull Fac Sci Assiut Univ 19:37–60

Ahmed AH, Habtoor A (2015) Heterogeneously depleted Precambrian lithosphere deduced from mantle peridotites and associated chromitite deposits of Al'Ays ophiolite, Northwestern Arabian Shield, Saudi Arabia. Ore Geol Rev 67:279–296

Ahmed AH, Arai S, Attia A (2001) Petrological characteristics of podiform chromitites and associated peridotites of the Pan African Proterozoic ophiolite complexes of Egypt. Miner Deposita 36:72–84

Ahmed AH, Gharib ME, Arai S (2012) Characterization of the thermally metamorphosed mantle–crust transition zone of the Neoproterozoic ophiolite at Gebel Mudarjaj, south Eastern Desert, Egypt. Lithos 142–143:67–83

Andresen A, Abu El-Rus MA, Myhre PI, Boghdady GY, Coru F (2009) U-Pb TIMS age constraints on the evolution of the Neoproterozoic Meatiq Gneiss Dome, Eastern Desert, Egypt. Int J Earth Sci 98:481–497

Anzil PA, Guereschi AB, Martino RD (2012) Mineral chemistry and geothermometry using relict primary minerals in the La Cocha ultramafic body: a slice of the upper mantle in the Sierra Chica of Cordoba, Sierras Pampeanas, Argentina. J S Am Earth Sci 40:38–52

Arai S (1992) Chemistry of chromian spinel in volcanic rocks as a potential guide to magma chemistry. Mineral Mag 56:173–184

Arai S (1994) Compositional variation of olivine-chromain spinel in Mg-rich magmas as a guide to their residual spinel peridotites. J Volcanol Geoth Res 59:279–294

Azer MK, Khalil AES (2005) Petrological and mineralogical studies of Pan-African serpentinites at Bir Al-Edeid area, central Eastern Desert, Egypt. J Afr Earth Sci 43:525–536

Azer MK, Stern RJ (2007) Neoproterozoic (835–720 Ma) serpentinites in the Eastern Desert, Egypt: fragments of fore-arc mantle. J Geol 115:457–472

Azer MK, Samuel MD, Ali KA, Gahlan HA, Stern RJ, Ren M, Moussa HE (2013) Neoproterozoic ophiolitic peridotites along the Allaqi–Heiani Suture, South Eastern Desert, Egypt. Mineral Petrol 107(5):829–848

Aziz NRH, Aswad KJA, Koyi HA (2011) Contrasting settings of serpentinite bodies in the northwestern Zagros Suture Zone, Kurdistan region, Iraq. Geol Mag 148:819–837

Barnes SI (2000) Chromite in Komatiites, II. Modification during Greenschist to Mid Amphibolite Facies Metamorphism. J Petrol 41:387–409

Beccaluva L, Macciota G, Piccardo GB, Zeda O (1989) Clinopyroxene composition of ophiolitic basalts as petrogenetic indicator. Chem Geol 77:165–182

Bloomer SH, Taylor B, Macleod CJ et al. (1995) Early arc volcanism and ophiolite problem: a perspective from drilling in the Western Pacific. In: Taylor B, Natland J (eds) Active margins and marginal basins of the western Pacific. Geophys Monogr 88: 1–30

Bodinier JL, Godard M (2003) Orogenic, ophiolitic, and abyssal peridotites. In: Carlson RW (ed), Treatise on geochemistry mantle and core: treatise on geochemistry, 2 edn. Elsevier Science Ltd, Amsterdam, pp 103–170

Bonatti E, Michael PJ (1989) Mantle peridotites from continental rifts to oceanic basins to subduction zones. Earth Planet Sci Lett 91:297–311

Boskabadi A, Pitcairn IK, Broman C, Boyce A, Teagle DAH, Cooper MJ, Azer MK, Stern RJ, Mohamed FH, Majka J (2017) Carbonate alteration of ophiolitic rocks in the Arabian-Nubian Shield of Egypt: sources and compositions of the carbonating fluid and implications for the formation of Au deposits. Int Geol Rev 59(4):391–419

Chalot-Prat F, Ganne J, Lombard A (2003) No significant element transfer from the oceanic plate to the mantle wedge during subduction and exhumation of the Tethys lithosphere (Western Alps). Lithos 69:69–103

Choi SH, Shervais JW, Mukasa SB (2008) Supra-subduction and abyssal mantle peridotites of the coast range ophiolite, California. Contrib Miner Petrol 156:551–576

Dai J, Wang C, Hébert R, Santosh M, Li Y, Xu J (2011) Petrology and geochemistry of peridotites in the Zhongba ophiolite, Yarlung Zangbo Suture Zone: implications for the Early Cretaceous intraoceanic subduction zone within the Neo-Tethys. Chem Geol 288:133–148

Dai J, Wang C, Polat A, Santosh M, Li Y, Ge Y (2013) Rapid forearc spreading between 130 and 120 Ma: evidence from geochronology and geochemistry of the Xigaze ophiolite, southern Tibet. Lithos 172–173:1–16

Delavari M, Amini S, Saccani E, Beccaluva L (2009) Geochemistry and petrogenesis of mantle peridotites from the Nehbandan Ophiolitic Complex, eastern Iran. J App Sci 9(15):2671–2687

Deschamps F, Guillot S, Godard M, Chauvel C, Andreani M, Hattori K (2010) In situ characterization of serpentinites from forearc mantle wedges: timing of serpentinization and behavior of fluid-mobile elements in subduction zones. Chem Geol 269:262–277

Deschamps F, Godar M, Guillot S, Hattori K (2013) Geochemistry of subduction zone serpentinites: a review. Lithos 178:96–127

Dick HJ, Bullen T (1984) Chromian spinel as a petrogenetic indicator in abyssal and alpine type peridotites and spatially associated lavas. Contrib Mineral Petrol 86:51–76

El Bahariya GA (2008) Geology, mineral chemistry and petrogenesis of Neoproterozoic metamorphosed ophiolitic ultramafics, Central Eastern Desert, Egypt: implication for the classification and origin of the ophiolitic mélange. Egypt J Geol 52:55–81

El Bahariya GA (2012) Classification and origin of the Neoproterozoic ophiolitic mélanges in the Central Eastern Desert of Egypt. Tectonophysics 568:357–370

El Bahariya GA, Arai S (2003) Petrology and origin of Pan-African serpentinites with particular reference to chromian spinel compositions, Eastern Desert, Egypt: implication for supra-subduction zone ophiolite. Third International Conference on the Geology of Africa, Assiut University, Egypt, 371–388

El-Bayoumi R (1980) Ophiolites and associated rocks of Wadi Ghadir, East of Gebel Zabara, Eastern Desert, Egypt. Ph.D. thesis, Cairo University

El-Gaby S (2005) Integrated evolution and rock classification of the Pan-African belt in Egypt. First symposium on the classification of the basement complex of Egypt. Bull Fac Sci, Assiut University, 1–9

El-Sayed MM, Furnes H, Mohamed FH (1999) Geochemical constraints on the tectonomagmatic evolution of the late Precambrian Fawakhir ophiolite, central Eastern Desert, Egypt. J Afr Earth Sci 29:515–533

El-Sharkawy MA, El-Bayoumi R (1979) The ophiolites of Wadi Ghadir area, Eastern Desert, Egypt. Ann Geol Surv Egypt 9:125–135

Evans B, Frost B (1975) Chrome spinel in progressive metamorphism: a preliminary analysis. Geochim Cosmochim Acta 39:379–414

Farahat ES (2008) Chrome spinels in serpentinites and talc carbonates of the El-Ideid–El Sodmein District, central Eastern Desert, Egypt: their metamorphism and petrogenetic implications. Chem Erde 68(2):195–205

Farahat ES, El Mahallawi MM, Hoinkes G, Abdel Aal AY (2004) Continental back-arc basin origin of some ophiolites from the Eastern Desert of Egypt. Mineral Petrol 82:81–104

Farahat ES, Hoinkes G, Mogessie A (2011) Petrogenetic and geotectonic significance of Neoproterozoic suprasubduction mantle as revealed by the Wizer ophiolite complex, Central Eastern Desert, Egypt. Int J Earth Sci 100:1433–1450

Floyd PA (1991) Oceanic basalts. Blachie and Son Ltd, New York

Frey FA, Suen JC, Stockman HW (1985) The Ronda high temperature peridotite: geochemistry and petrogenesis. Geochim Cosmochim Acta 49:2469–2491

Ghoneim MF, Salem IA, Hamdy MM (2003) Origin of magnesite veins in serpentinites from Mount El-Rubshi and Mount El-Maiyit, Eastern Desert, Egypt. Arch Mineral 54:41–63

Godard M, Lagabrielle Y, Alard O, Harvey J (2008) Geochemistry of the highly depleted peridotites drilled at ODP Sites 1272 and 1274 (Fifteen-Twenty Fracture Zone, Mid-Atlantic Ridge): implications for mantle dynamics beneath a slow spreading ridge. Earth Planet Sci Lett 267:410–425

Gruau G, Bernard-Griffiths J, Lécuyer C (1998) The origin of U-shaped rare earth patterns in ophiolite peridotites: assessing the role of secondary alteration and melt/rock reaction. Geochim Cosmochim Acta 62(21/22):3545–3560

Guillot S, Hattori KH, de Sigoyer J, Nägler T, Auzende AL (2001) Evidence of hydration of the mantle wedge and its role in the exhumation of eclogites. Earth Planet Sci Lett 193:115–127

Hamdy MM, Lebda EM (2007) Metamorphism of ultramafic rocks at Gebel Arais and Gebel Malo Grim, Eastern Desert, Egypt: mineralogical and O-H stable isotopic constraints. Egypt J Geol 51:105–124

Hart SR, Zindler A (1986) In search of a bulk-Earth composition. Chem Geol 57:247–267

Hassanen MA (1985) Petrology and geochemistry of ultramafic rocks in the Eastern Desert, Egypt, with special reference to Fawakhir area. Ph.D. dissertation. Alexandria University, Egypt

Hattori KH, Guillot S (2007) Geochemical character of serpentinites associated with high- to ultrahigh-pressure metamorphic rocks in the Alps, Cuba, and the Himalayas: recycling of elements in subduction zones. Geochem Geophys Geosyst. https://doi.org/10.1029/2007GC001594

Hawkins JW (2003) Geology of supra-subduction zones—implications for the origin of ophiolites. In: Dilek Y, 438 Newcomb S (eds) Ophiolite Concept and the Evolution of Geological Thought. Boulder, CO, Geological 439 Society of America Special Paper 373: 227–268

Hellebrand E, Snow JE, Dick HJB, Hofmann AW (2001) Coupled major and trace elements as indicators of the extent of melting in mid-ocean-ridge peridotites. Nature 410:677–681

Ishii T, Robinson PT, Maekawa H, Fiske R (1992) Petrological studies of peridotites from diapiric Serpentinite Seamounts in the Izu-Ogasawara-Mariana forearc, leg 125. In: Pearce J, Stokking LB, et al (eds), Proceedings of the Ocean Drilling Project, Leg 125, Scientific Results (College Station), pp 445–485

Jagoutz E, Palme H, Baddenhausen H, Blum K, Cendales M, Dreibus G, Spettel B, Lorenz V, Wanke H (1979) The abundances of major, minor and trace elements in the earth's mantle as derived from primitive ultramafic nodules. Proc. Lunar Planet. Conf. 10: 2031–2050

Johnson PR, Abdelsalam MG, Stern RJ (2003) The Bi'r Umq-Nakasib suture zone in the Arabian-Nubian Shield: a key to understand crustal growth in the East African Orogen. Gondwana Res 6:523–530

Kamenetsky VS, Crawford AJ, Meffre S (2001) Factors controlling chemistry of magmatic spinel: an empirical study of associated olivine, Cr-spinel and melt inclusions from primitive rocks. J Petrol 42:655–671

Khalil KI (2007) Chromite mineralization in ultramafic rocks of the Wadi Ghadir area, Eastern Desert, Egypt: mineralogical, microchemical and genetic study. Neues Jb Mineral Abh 183:283–296

Khalil AES, Azer MK (2007) Supra-subduction affinity in the Neoproterozoic serpentinites in the Eastern Desert, Egypt: evidence from mineral composition. J Afr Earth Sci 49:136–152

Khedr MZ, Arai S (2013) Origin of Neoproterozoic ophiolitic peridotites in south Eastern Desert, Egypt, constrained from primary mantle mineral chemistry. Mineral Petrol 107(5):807–828

Khedr MZ, Arai S, Python M, Tamura A (2014) Chemical variations of abyssal peridotites in the central Oman ophiolite: evidence of oceanic mantle heterogeneity. Gondwana Res 25:1242–1262

Khudeir AA (1995) Chromian spinel-silicate chemistry in peridotite and orthopyroxenite relicts from ophiolitic serpentinites, Eastern Desert, Egypt. Bull Fac Sci Assiut Univ 24:221–261

Khudeir AA, El Haddad MA, Leake BE (1992) Compositional variation in chromite from the Eastern Desert. Mineral Mag 56:567–574

Kodolányi J, Pettke T, Spandler C, Kamber BS, Gméling K (2012) Geochemistry of ocean floor and fore-arc serpentinites: constraints on the ultramafic input to subduction zones. J Petrol 53:235–270

Le Bas MJ (1962) The role of aluminum in igneous clinopyroxenes with relation to their parentage. Am J Sci 260:267–288

McDonough WF, Sun SS (1995) The composition of the Earth. Chem Geol 120:223–253

Mellini M, Rumori C, Viti C (2005) Hydrothermally reset magmatic spinels in retrograde serpentinites: formation of "ferritchromit" rims and chlorite aureoles. Contrib Miner Petrol 149:266–275

Mével C (2003) Serpentinization of abyssal peridotites at mid-ocean ridges. C R Geosci 335:825–852

Mondal SK, Baidya TK, Rao KNG, Glascock MD (2001) PGE and Ag mineralization in a breccia zone of the Precambrian Nuasahi Ultramafic–mafic Complex, Orissa, India. Can Mineral 39:979–996

Morimoto NFJ, Ferguson AK, Ginzburg IV, Ross M, Seifert FA, Zussmaann I (1988) Nomenclature of pyroxene. Mineral Mag 52:535–550

Niu Y (2004) Bulk-rock major and trace element compositions of abyssal peridotites: implications for mantle melting melt extraction and post-melting processes beneath mid-ocean ridges. J Petrol 45(12):2423–2458

Nozaka T (2010) A note on compositional variation of olivine and pyroxene in thermally metamorphosed ultramafic complexes from SW Japan. Okayama Univ Earth Sci Rep 17(1):1–5

O'Hanley DS (1996) Serpentinites, records of tectonic and petrological history. Oxford Monographs on Geology and Geophysics no 34

Obeid MA, Khalil AES, Azer MK (2016) Mineralogy, geochemistry and geotectonic significance of the Neoproterozoic ophiolite of Wadi Arais area, south Eastern Desert, Egypt. Int Geol Rev 58:687–702

Ohara Y, Stern RJ, Ishii T, Yurimoto H, Yamazaki T (2002) Peridotites from the Mariana Trough: first look at the mantle beneath an active back-arc basin. Contrib Mineral Petrol 143:1–18

Ozawa K (1994) Melting and melt segregation in the mantle wedge above a subduction zone; evidence from the chromite-bearing peridotites of the Miyamori ophiolite complex, northeastern Japan. J Petrol 35:647–678

Parkinson IJ, Arculus RJ (1999) The redox state of subduction zone: insights from arc peridotites. Chem Geol 160:409–423

Parkinson IJ, Pearce JA (1998) Peridotites from the Izu–Bonin–Mariana fore-arc (ODP Leg125): evidence for mantle melting and meltmantle interaction in a supra-subduction zone setting. J Petrol 39:1577–1618

Paulick H, Bach W, Godard M, De Hoog JCM, Suhr G, Harvey J (2006) Geochemistry of abyssal peridotites (Mid-Atlantic Ridge, 15°20′N, ODP Leg 209): implications for fluid/rock interaction in slow spreading environments. Chem Geol 234:179–210

Pearce JA, Barker PF, Edwards SJ, Parkinson IJ, Leat PT (2000) Geochemistry and tectonic significance of peridotites from the south sandwich arc-basin system, South Atlantic. Contrib Miner Petrol 139:36–53

Roeder PL (1994) Chromite from the Fiery rain of Chondrules to the Kilauea iki lava lake. Canad Mineral 32:729–746

Rollinson H, Adetunji J (2015) The geochemistry and oxidation state of podiform chromitites from the mantle section of the Oman ophiolite: a review. Gondwana Res 27:543–554

Sack RO, Ghiorso MS (1991) Chromian spinels as petrogenetic indicators: thermodynamic and petrological applications. Am Miner 76:827–847

Salters VJM, Stracke A (2004) Composition of the depleted mantle. Geochem Geophys Geosyst. https://doi.org/10.1029/2003GC000597

Sano S, Kimura JI (2007) Clinopyroxene REE geochemistry of the Red Hills peridotite, New Zealand: interpretation of magmatic processes in the upper mantle and in the Moho transition zone. J Petrol 48:113–139

Savov IP, Ryan JG, D'Antonio M, Kelley K, Mattie P (2005a) Geochemistry of serpentinized peridotites from the Mariana Forearc Conical Seamount, ODP Leg 125: implications for the elemental

recycling at subduction zones. Geochem Geophys Geosyst. https://doi.org/10.1029/2004GC000777

Savov IP, Guggino S, Ryan JG, Fryer P, Mottl MJ (2005b) Geochemistry of serpentinite muds and metamorphic rocks from the Mariana forearc, ODP Sites 1200 and 778–779, South Chamorro and Conical Seamounts. In: Shinohara M, Salisbury MH, Richter C (eds), Proceedings of the Ocean Drilling Program, Scientific Results 195: 1–49

Shackleton RM (1994) Review of late proterozoic sutures, ophiolitic mélanges and tectonics of eastern Egypt and northeast Sudan. Geol Rundsch 83:537–546

Shackleton RM, Ries AC, Graham RH, Fitches WR (1980) Late Precambrian ophiolitic mélange in the Eastern Desert of Egypt. Nature 285:472–474

Sharma M, Wasserburg GJ (1996) The neodymium isotopic compositions and rare earth patterns in highly depleted ultramafic rocks. Geochim Cosmochim Acta 60:4537–4550

Snow JE, Dick HJB (1995) Pervasive magnesium loss by marine weathering of peridotite. Geochim Cosmochim Acta 59:4219–4235

Song S, Su L, Niu Y, Lai Y, Zhang L (2009) CH4 inclusions in orogenic harzburgite: evidence for reduced slab fluids and implication for redox melting in mantle wedge. Geochim Cosmochim Acta 73(6):1737–1754

Stern RJ (1994) Arc assembly and continental collision in the Neoproterozoic East African Orogen: implications for the consolidation of Gondwanaland. Ann Rev Earth Planet Sci 22:319–351

Stern RJ (2004) Subduction initiation: spontaneous and induced. Earth Planet Sci Lett 226:275–292

Stern RJ, Gwinn CJ (1990) Origin of late Precambrian intrusive carbonates, Eastern Desert of Egypt and Sudan: C, O, and Sr isotopic evidence. Precambr Res 46:259–272

Stern RJ, Johanson PR, Kröner A, Yibas B (2004) Neoproterozoic ophiolites of the Arabian-Nubian Shield. In: Kusky TM (ed), Precambrian ophiolites and related rocks. Developments in Precambrian geology, vol. 13. Elsevier, Amsterdam, pp 95–128

Suita M, Strieder A (1996) Cr-spinels from Brazilian mafic–ultramafic complexes: metamorphic modifications. Int Geol Rev 38(3):245–267

Uysal I, Yalçın Ersoy E, Karslı O, Dilek Y, Burhan Sadıklar M, Ottley CJ, Tiepolo M, Meisel T (2012) Coexistence of abyssal and ultra-depleted SSZ type mantle peridotites in a Neo-Tethyan Ophiolite in SW Turkey: constraints from mineral composition, whole-rock geochemistry (major–trace–REE–PGE), Re–Os isotope systematics. Lithos 132–133:50–69

Yang S-H, Zhou M-F (2009) Geochemistry of the ~ 430–Ma Jingbulake mafic–ultramafic intrusion in Western Xinjiang, NM China: implications for subduction related magmatism in the South Tianshan orogenic belt. Lithos 113: 259–273

Zimmer M, Kröner A, Jochum KP, Reischmann T, Todt W (1995) The Gabal Gerf complex: a Precambrian 600 N-MORB ophiolite in the Nubian Shield, NE Africa. Chem Geol 123:29–51